UCSF

Title

Targeting iron metabolism in high-grade glioma with 68Ga-citrate PET/MR

Permalink

https://escholarship.org/uc/item/5s5344s8

Journal

JCI Insight, 3(21)

ISSN

2379-3708

Authors

Behr, Spencer C
Villanueva-Meyer, Javier E
Li, Yan
et al.

Publication Date

2018-11-02

DOI

10.1172/jci.insight.93999

Peer reviewed

Targeting iron metabolism in high-grade glioma with 68Ga-citrate PET/MR

Spencer C. Behr,[1] Javier E. Villanueva-Meyer,[1] Yan Li,[1] Yung-Hua Wang,[1] Junnian Wei,[1] Anna Moroz,[1,2] Julia K.L. Lee,[1] Jeffrey C. Hsiao,[1] Kenneth T. Gao,[1] Wendy Ma,[1] Soonmee Cha,[1] David M. Wilson,[1] Youngho Seo,[1] Sarah J. Nelson,[1,3,4] Susan M. Chang,[3,5] and Michael J. Evans[1,3,6]

[1]Department of Radiology and Biomedical Imaging, UCSF, San Francisco, California, USA. [2]Skolkovo Institute of Science and Technology, Skolkovo Innovation Center, Moscow, Russia. [3]Helen Diller Family Comprehensive Cancer Center, [4]Department of Bioengineering and Therapeutic Sciences, [5]Department of Neurological Surgery, and [6]Department of Pharmaceutical Chemistry, UCSF, San Francisco, California, USA.

Noninvasive tools that target tumor cells could improve the management of glioma. Cancer generally has a high demand for Fe(III), an essential nutrient for a variety of biochemical processes. We tested whether 68Ga-citrate, an Fe(III) biomimetic that binds to apo-transferrin in blood, detects glioma in preclinical models and patients using hybrid PET/MRI. Mouse PET/CT studies showed that 68Ga-citrate accumulates in subcutaneous U87MG xenografts in a transferrin receptor–dependent fashion within 4 hours after injection. Seventeen patients with WHO grade III or IV glioma received 3.7–10.2 mCi 68Ga-citrate and were imaged with PET/MR 123–307 minutes after injection to establish that the radiotracer can localize to human tumors. Multiple contrast-enhancing lesions were PET avid, and tumor to adjacent normal white matter ratios were consistently greater than 10:1. Several contrast-enhancing lesions were not PET avid. One minimally enhancing lesion and another tumor with significantly reduced enhancement following bevacizumab therapy were PET avid. Advanced MR imaging analysis of one patient with contrast-enhancing glioblastoma showed that metabolic hallmarks of viable tumor spatially overlaid with 68Ga-citrate accumulation. These early data underscore that high-grade glioma may be detectable with a radiotracer that targets Fe(III) transport.

Introduction

Imaging plays a crucial role in the management of brain tumor patients. Given its widespread availability, high spatial resolution, and excellent soft tissue contrast, structural MRI is the mainstay for neuro-oncologic diagnosis, treatment planning, and follow-up. However, conventional MR techniques have several important limitations (1). For example, contrast enhancement, a marker of blood-brain barrier permeation, is neither sensitive nor specific for the presence of viable tumor. Moreover, the generally low specificity of MR for tumor-associated changes at the molecular level makes it challenging to understand underlying tumor biology (2). As a result, there is a compelling need to develop molecular imaging technologies that can noninvasively characterize glioma pathophysiology for improved diagnosis and to better direct therapy.

Our increasing understanding of glioma tumorigenesis has fostered the development of several molecular imaging strategies intended to more specifically visualize tumor burden. The most well-studied PET approaches in glioma target glycolytic flux using 18F-fluorodeoxyglucose (FDG); glutamine metabolism with 4-[18F]-(2S,4R)-fluoroglutamine (18F-Gln); amino acid metabolism using 11C-methionine (MET), 18F-fluoroethyltyrosine (FET), and 3,4-dihydroxy-6-[18F]-fluoro-L-phenylalanine (FDOPA); lipid metabolism using 11C-choline; and hypoxia using 18F-fluoromisonidazole (FMISO) (3, 4). Many of these radiotracers better delineate malignant cells compared with 18F-FDG, which does not detect malignant tissue with a high degree of sensitivity or specificity and has high background brain uptake. However, those radiotracers that have been evaluated after chemoradiation also have shown uptake in nonmalignant processes, and their specificity for cancer is currently estimated to be between 60% and 90% (5–8).

In considering alternative imaging strategies for glioma, we noted that cancer cells generally have an elevated demand for Fe(III), an essential nutrient required for various biochemical processes associated with cell growth and proliferation (9). We and others have also shown that pathobiological events common
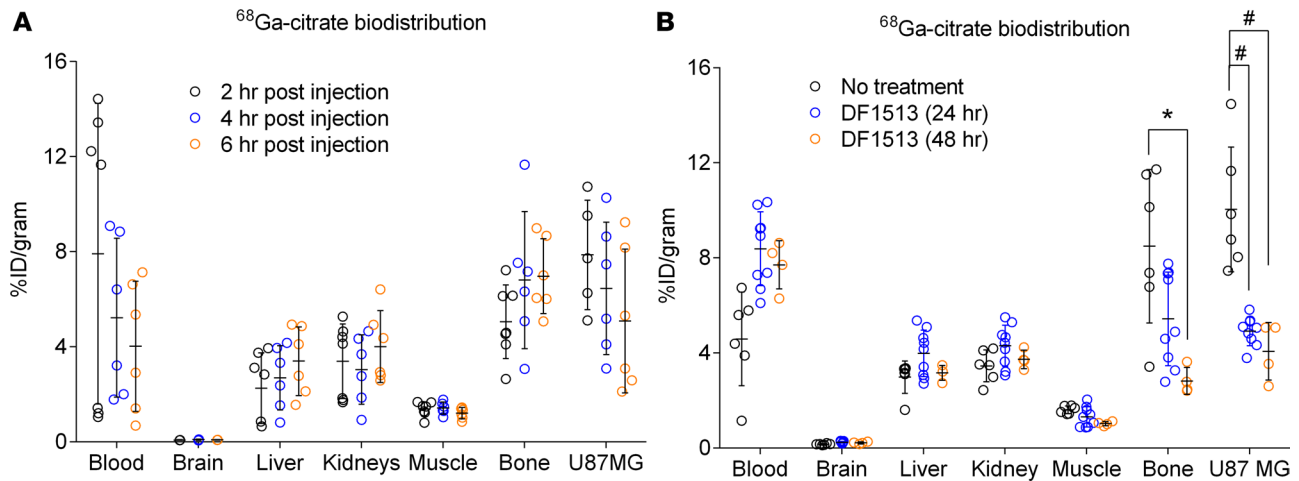
Figure 1. Preclinical data showing that ⁶⁸Ga-citrate uptake is TFRC dependent in glioblastoma tumors in vivo. (A) A biodistribution study showing the accumulation of ⁶⁸Ga-citrate in normal mouse tissues and subcutaneous U87 MG tumors at 2, 4, and 6 hours after injection. Tumor-bearing *nu/nu* mice (*n* = 6/time point) received ~400 µCi ⁶⁸Ga-citrate via tail vein. Peak radiotracer uptake was observed in the tumors at 4 hours after injection. The data were reproduced in 2 independent animal cohorts, and the cumulative data are represented in the figure. **(B)** Ex vivo biodistribution data from selected tissues showing the effect on ⁶⁸Ga-citrate biodistribution due to co-administration of an anti-TFRC antibody that disrupts the interaction between Tf and TFRC. Intact male *nu/nu* mice bearing subcutaneous U87 MG tumors (*n* = 4–7/treatment arm) received ⁶⁸Ga-citrate (~400 µCi/mouse) or ⁶⁸Ga-citrate (~400 µCi/mouse) 24 hours after administration of 100 µg DF1535, a monoclonal antibody (IgG) that binds an extracellular epitope on TFRC and disrupts Tf uptake into cells in vitro. The biodistribution data were collected 4 hours after injection of ⁶⁸Ga-citrate. Approximately 50% of the ⁶⁸Ga-citrate accumulation in the tumors was suppressed by DF1513 (#*P* < 0.01), underscoring that ⁶⁸Ga-citrate localizes to tumors by binding Tf in situ. Moreover, radiotracer accumulation was higher in the blood pool of mice treated with DF1513, consistent with a model in which ⁶⁸Ga-citrate exists in the blood bound to a large biomolecule (MW of Tf, ~80 kDa). Last, radiotracer uptake was competed with DF1513 in the bone (*P* < 0.01). Overall, these data show that ⁶⁸Ga accumulates in tumors within 4 hours after injection in a TFRC-dependent fashion. Statistically significant differences were calculated using an unpaired, 2-tailed Student's *t* test. The data were reproduced in an additional animal cohort. Horizontal lines are placed to bridge the treatment arms for which a Student's *t* test was applied to determine statistical significance.

to high-grade glioma, most notably mTORC1 hyperactivity, can increase Fe(III) uptake into cancer cells by upregulating the activity of the transferrin (Tf) receptor (TFRC) in preclinical models (10–14). On this basis, we evaluated whether ⁶⁸Ga-citrate, a radiometal for PET that like Fe(III) binds to Tf in vivo (15, 16), can detect high-grade glioma using combined PET and MRI modalities.

Results

We first studied the biokinetics and biodistribution of ⁶⁸Ga-citrate in mice bearing subcutaneous glioma tumors. Intact male *nu/nu* mice were inoculated with U87 MG tumors (a PTEN-null model of glioblastoma) and treated with ~400 µCi of ⁶⁸Ga-citrate (Figure 1A and Supplemental Figure 1). Biodistribution studies showed peak tumor uptake at 2–4 hours after injection (7.27% ± 1.8% injected dose [ID]/g and 6.95% ± 2.2% ID/g). ⁶⁸Ga accumulation in the normal brain was low at all time points (e.g., 0.15% ± 0.07% ID/g at 4 hours). Low radiotracer accumulation was observed in all normal tissues, with the exception of the bone (e.g., 7.08% ± 2.7% ID/g). At 4 hours after injection, the tumor to brain, tumor to muscle, and tumor to blood ratios were 46.5, 4.8, and 1.3, respectively.

To test whether ⁶⁸Ga uptake in the tumor is dependent on TFRC activity at 4 hours after injection, a separate cohort of mice bearing U87 MG tumors were treated with vehicle or DF1513, an anti-TFRC IgG that blocks the cellular uptake of ¹²⁵I-labeled human holo-Tf in vitro (Supplemental Figure 2, A and B). Administration of DF1513 (100 µg) via tail vein injection 24 or 48 hours prior to the injection of ⁶⁸Ga-citrate resulted in a significant reduction in tumor uptake of the radiotracer (see Figure 1B and Supplemental Figure 2B). Moreover, radiotracer uptake was competed in the bone compartment.

Our preclinical data and prior experience with ⁶⁸Ga-citrate PET in prostate cancer and hepatocellular carcinoma patients showed that at least 2 hours of uptake time after injection was required to visualize human tumors (17, 18). On this basis, the first patient was scanned 123 minutes after injection with 6.9 mCi ⁶⁸Ga-citrate. Several contrast-enhancing lesions were determined to be avid for the radiotracer (maximum standardized uptake value [SUV_max], 1.4, 2.2, 2.2; see Supplemental Table 1). To assess the temporal uptake of radiotracer, the PET data from the first 5 patients were reconstructed into 3 time points. The first time point was reconstructed from 0 to 15 minutes, the second time point from 25 to 40 minutes, and the final
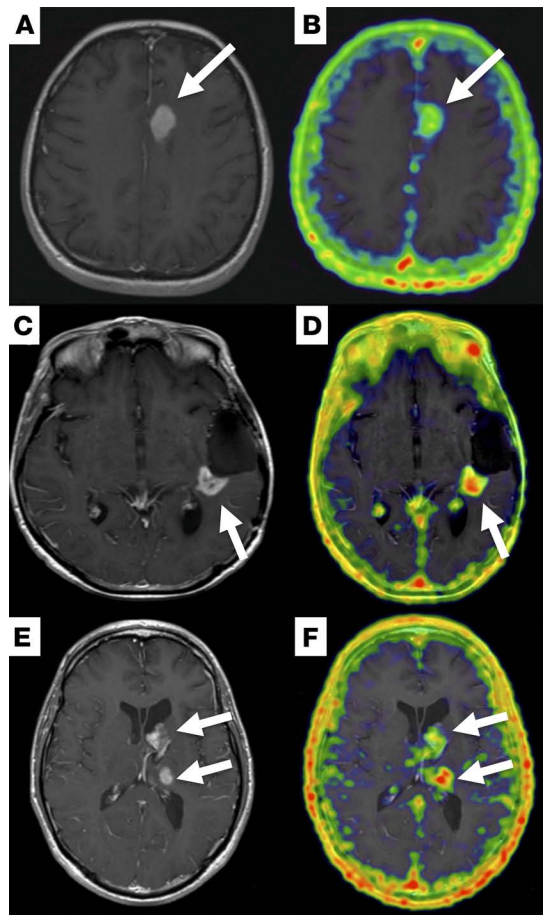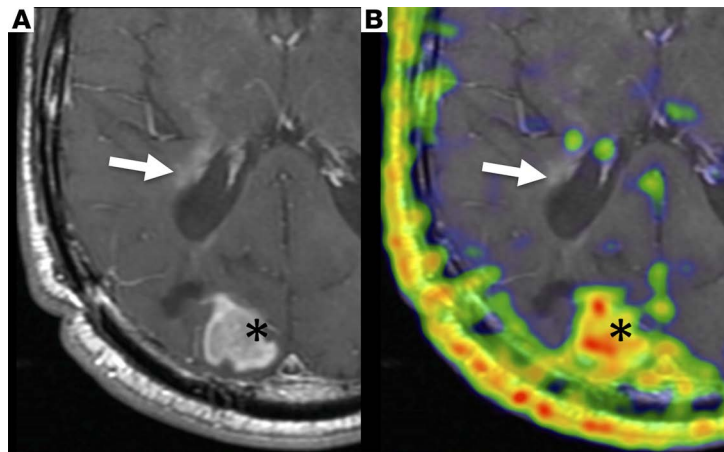
Figure 2. Post-contrast T1-weighted MR and fused ^{68}Ga-citrate PET/MR images in 3 different patients with high-grade glioma. Representative post-contrast T1-weighted MR (**A**, **C**, and **E**) and fused PET/MR (**B**, **D**, and **F**) images are shown. (**A** and **B**) 38-year-old woman with glioblastoma: PET/MR images acquired 300 minutes after injection of 6.9 mCi (255.3 MBq) ^{68}Ga-citrate show focal radiotracer uptake (SUV$_{max}$, 2.7) corresponding to the enhancing left frontal mass (white arrows). (**C** and **D**) 62-year-old woman with recurrent glioblastoma: PET/MR images acquired 260 minutes after injection of 10 mCi (370 MBq) ^{68}Ga-citrate show focal radiotracer uptake (SUV$_{max}$, 2.7) corresponding to an enhancing mass along the resection bed (white arrows). (**E** and **F**) 32-year-old man with glioblastoma: PET images acquired 264 minutes after injection of 3.5 mCi (129.5 MBq) ^{68}Ga-citrate show uptake in the two enhancing lesion in the left thalamus (SUV$_{max}$, 3.5) and left caudate head (SUV$_{max}$, 2.9, white arrows).

time point from 50 to 60 minutes. SUV$_{max}$ of the avid lesions were recorded by drawing an identically sized volumes of interest (VOI) in the same location at each time point. SUV$_{mean}$ was recorded in the blood pool and white matter by drawing a 1-cm VOI in the same location at each time point. Longitudinal analysis of radiotracer uptake from 2.0 to 4.5 hours after injection showed that the ratio of tumor to white matter and tumor to blood pool was generally highest at 3.5–4.5 hours uptake time (Supplemental Table 2). Extending these parameters, a total of 23 PET/MR examinations were performed in 17 patients, with 6 patients receiving repeat PET/MR examinations. The average age of the cohort was 46 ± 13 years (range, 26–76). Twelve were male, and 5 were female. Seven patients harbored WHO grade III tumors and 10 harbored WHO grade IV tumors (Supplemental Table 1). All patients received between 3.7 and 10.2 mCi (136 and 377 MBq) of ^{68}Ga-citrate, although no visual improvement in the quality of the PET scan was observed with increasing dose.

Inter-rater reliability for imaging findings met the criteria to be defined as "near-perfect" for (i) contrast enhancement (κ = 0.829), (ii) radiotracer uptake (κ = 0.889), and (3) discordance between MRI contrast enhancement and radiotracer uptake (κ = 1). Radiotracer uptake in the evaluated normal structures was consistently low, and uptake in the normal white matter was extremely low (SUV$_{mean}$, 0.01 ± 0.02; see Supplemental Table 3). Despite increasing doses, there was no significant qualitative improvement of image quality observed above 3.7 mCi.

Lesions could be generally classified as (i) matching PET uptake with contrast enhancement, (ii) MR discordant (MR contrast enhancement without PET uptake), and (iii) PET discordant (PET uptake without MR contrast enhancement). A total of 44 lesions were identified on either the PET or after contrast MR. Twenty-eight lesions had matching PET uptake and MR enhancement (Figure 2). The average size was 2.2 ± 1.05 cm (range, 0.5–4.5 cm), with an SUV$_{max}$ of 2.17 ± 1.02 (range, 0.3–4.3). Two lesions had areas of MR enhancement greater than PET (Figure 3). The average size was 2.75 ± 0.07 cm (range, 2.7–2.8), with an SUV$_{max}$ of 0.7 ± 0.28 (range, 0.5–0.6). Ten lesions were seen on MR only, with an average size of 0.93 ± 0.79 cm (range, 0.3–2.9 cm). One PET-avid lesion had no clear enhancement on MR,

Figure 3. An example of enhancing lesion on MR without ^{68}Ga-citrate uptake. Post-contrast T1-weighted MR (**A**) images and fused PET/MR (**B**) images in a 50-year-old male with glioblastoma. The PET/MR study, performed 180 minutes after injection of 5.8 mCi (214.6 MBq) ^{68}Ga-citrate, shows matching radiotracer uptake (SUV$_{max}$, 4.3) within a homogeneously enhancing right occipital mass (*). A second enhancing lesion in the periventricular white mater (white arrows) does not associate with any ^{68}Ga-citrate uptake.

with an SUV$_{max}$ of 3.5 and a tumor to white matter ratio of 185:1. Four lesions were seen on MR without corresponding PET uptake (Figure 4). The average SUV$_{max}$ was 2.01 ± 1.09 (range, 0.3 to 4.3) and SUV$_{peak}$ was 1.18 ± 0.66 (range, 0.1–2.6; see also Supplemental Table 4). The ratio of tumor to white matter SUV was >10:1 for all lesions.

Six patients underwent repeat PET/MR examinations — 2 had WHO grade III tumors and 4 had WHO grade IV tumors. Radiotracer uptake in normal structures was consistent between scans (Supplemental Table 5). One patient had decreased enhancing tumor burden after treatment with bevacizumab on both PET and MRI (Figure 5). This patient had 2 lesions both prior to and following therapy that showed a decrease in MR size by –29.5%, and a change in SUV$_{max}$ of –70.2% and SUV$_{peak}$ of –77.1%. In the same patient, a nonenhancing region within the site of an enhancing pretreatment tumor had persistent avidity for ^{68}Ga-citrate (Figure 4).

One of the patients who underwent repeat imaging had a WHO grade IV tumor that did not appear on PET or MR on the follow-up scan. Four of the 5 remaining patients had MR findings indicative of progression on the follow-up PET/MR scan. Among these patients, the number of PET-avid lesions increased from 7 to 8, and the average percent increase in uptake among 3 patients was 38% (Figure 6).

We next performed multimodal, multiparametric ^{68}Ga-citrate PET/MR acquisition to determine, qualitatively, any concordance between advanced MR parameters and PET. In addition to the PET (acquired 264 minutes after injection of 3.5 mCi ^{68}Ga-citrate) and structural MR sequences, a 32-year-old man with glioblastoma was studied with 3D lactate-edited MR spectroscopy, arterial spin labeling perfusion, and diffusion tensor imaging (DTI; Figure 7). The study showed a left thalamic enhancing lesion with ^{68}Ga-citrate uptake (SUV$_{max}$ 4.0) corresponding to tumoral metabolism, including elevated choline to N-acetylaspartate (NAA) ratio and elevated perfusion.

Discussion

In this report, we show that high-grade glioma can be detected with ^{68}Ga-citrate, an Fe(III) biomimetic that binds to apo-Tf in blood. We demonstrated that ^{68}Ga-citrate uptake in preclinical tumor models is dependent on TFRC expression and activity, and then performed a clinical study that revealed 30 PET-avid lesions in 17 patients with WHO grade III or IV glioma. Importantly, the radiotracer uptake in normal white matter was essentially undetectable, and the tumor to adjacent white matter ratio was consistently ≥10:1 and at times exceeded 100:1. Moreover, approximately 20% of contrast-enhancing lesions were not avid for ^{68}Ga-citrate, showing that the radiotracer does not merely accumulate in regions of aberrant vasculature. ^{68}Ga-citrate PET also detected one minimally enhancing lesion, and a region with significantly reduced enhancement following treatment with bevacizumab. The variance in the SUV$_{mean}$ of normal tissues was low between repeat PET/MR acquisitions over 4–6 weeks. Finally, a preliminary study showed that regions of altered cellular metabolism detected on MR spectroscopy coincided with a PET-avid focus.
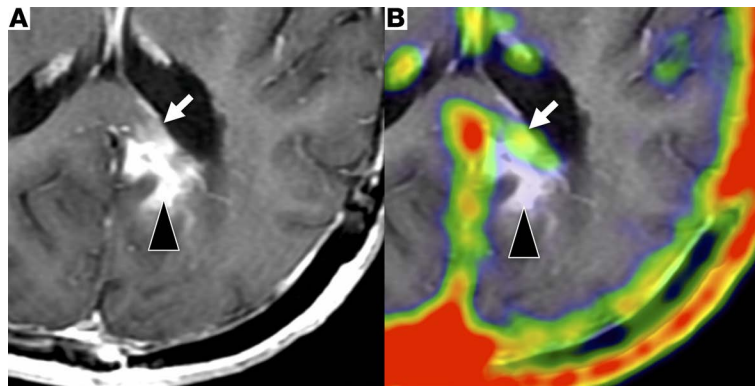
Figure 4. An example of discordant ^{68}Ga-citrate uptake and MR contrast enhancement. Post-contrast T1-weighted MR (**A**) and fused PET/MR (**B**) images in a 54 year-old female after treatment with bevacizumab for glioblastoma. PET images acquired 138 minutes after injection of 5.6 mCi (207.2 MBq) ^{68}Ga-citrate show discordant radiotracer and contrast enhancement in the left medial occipital region. Focal, low-level ^{68}Ga-citrate uptake (SUV$_{max}$, 0.5) corresponds to an area of faint enhancement (white arrows), while the adjacent area with more intense contrast enhancement is not associated with ^{68}Ga-citrate uptake (black arrowheads).

TFRC-independent mechanisms of gallium uptake have been proposed on the basis in vitro experiments in which cellular uptake of gallium can be induced with supraphysiological levels of endogenous nutrients (e.g., Ca^{2+}) (19). However, in vivo studies from the same group of investigators show that ^{67}Ga-citrate uptake is substantially reduced in vivo among virtually all normal tissues in hypotransferrinemic mice (20). Hypotransferrinemia did not reduce ^{67}Ga-citrate uptake in bone, but our blocking studies with the anti-TFRC mAb showed clear suppression of ^{68}Ga uptake in bone, or cells within the marrow.

Consistent with our preclinical data, prior studies with other forms of radiolabeled Tf also show that specific binding to TFRC is observable a few minutes to hours after injection. For example, Eckelman et al. reported specific binding of ^{18}F-labeled Tf to TFRC in normal baboon liver within 30 minutes after injection (21). Our prior studies with ^{89}Zr-labeled Tf have also shown that specific binding to the receptor is achieved in tumor and normal mouse tissues within 4 hours after injection (22). All of these findings are consistent with in vitro kinetic calculations showing rapid endocytosis and recycling of the Tf-TFRC complex (23, 24).

Acquiring tissue will be essential to establish the molecular determinants of high-grade glioma's avidity for ^{68}Ga-citrate, as well as the specificity of the radiotracer for cancer. Preclinical data suggest that Tf uptake in cancer cells can be linked to PI3K signaling pathway activation and/or MYC activity (11, 13, 17, 22, 25–27). Five of the 17 patients in this cohort had surgical tissue previously analyzed for EGFR overexpression, PTEN deletion, and MGMT methylation. Three patients were positive for PTEN deletion, and all of these patients had at least 1 PET-avid lesion. Of the 2 patients whose archival tissue was annotated as negative for PTEN deletion, one had PET-avid GBM, while the other had GBM that was not detected with PET. The patient with PET avid GBM was diagnosed and underwent surgery more than 20 years prior to the PET/MR, and the archival tissue may not reflect the molecular characteristics of the recurrent disease. A prospective study accruing patients with tissue from recent biopsy will likely be required to test a correlation between tumor signaling with SUV$_{max}$.

The tumor to normal brain ratio for ^{68}Ga-citrate is notably higher compared with other well-studied radiotracers. For instance, ^{18}F-FET, ^{11}C-MET, ^{18}F-FLT, ^{18}F-FDOPA, and ^{18}F-Gln consistently range between 2:1 and 4:1 (4, 28–30). The high tumor to normal brain ratio that we report in patients is driven by the exceedingly low uptake of ^{68}Ga-citrate in normal white and gray matter, and tumor uptake of the radiotracer is generally equivalent to that of the other metabolic radiotracers. Also, these radiotracers target discrete metabolic pathways in glioma. Therefore, a deeper understanding of the central oncogenes that promote the activation of the respective metabolic pathway may reveal unique clinical applications for the cognate radiotracer.

Atlas-based attenuation correction of the PET/MR images has quantification accuracy similar to that obtained from PET/CT. However, there are some inaccuracies around the paranasal sinuses (31), which may affect the PET quantification of lesions within the brain that are adjacent to theses structures. Studies with more esoteric MR sequences for cortical bone attenuation correction such as zero echo time (ZTE) are underway to determine whether these alternate attenuation correction algorithms can resolve this minor challenge.
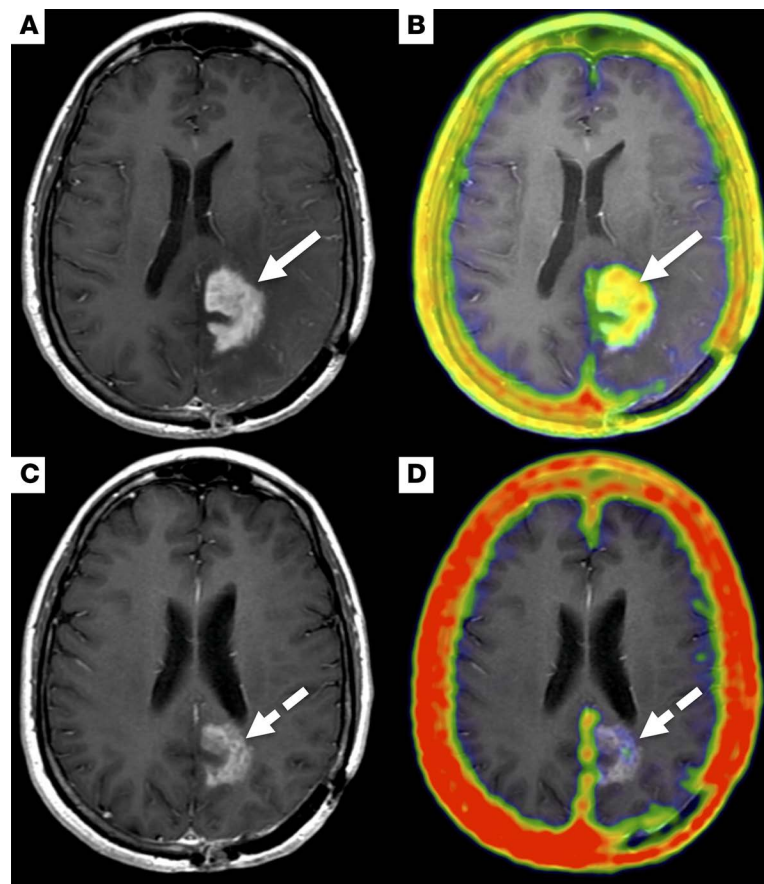
Figure 5. An example of treatment response detected on MR with a corresponding decline in ^{68}Ga-citrate uptake at the tumor. Pretreatment PET/MR images, T1-weighted post-contrast (**A**), and fused PET/MR images (**B**) acquired 140 minutes after injection of 5.6 mCi (207.2 MBq) ^{68}Ga-citrate show focal ^{68}Ga-citrate uptake (SUV$_{max}$, 2.3) that overlays with an enhancing mass in the left occipital lobe (white arrows). A follow-up PET/MR study was performed 6 weeks after the start of treatment with bevacizumab. The PET/MR acquisition was performed 240 minutes after injection of 7 mCi (259 MBq) ^{68}Ga-citrate. The T1-weighted post-contrast (**C**) and fused PET/MR (**D**) images show a decrease in both enhancement and ^{68}Ga-citrate uptake (SUV$_{max}$, 0.5) (dashed white arrows).

In conclusion, by combining ^{68}Ga-citrate PET with MRI on a hybrid scanner, we were able to localize high-grade gliomas. Further studies in patients undergoing image-guided tissue sampling or resection are needed to fully characterize the specificity of ^{68}Ga-citrate for tumor (^{68}Ga can be taken up by metabolically active leukocytes) and the molecular determinants of tumor avidity for this radiotracer.

Methods

General methods. The human glioblastoma cell lines U87 MG and U251 were purchased from ATCC and sub-cultured according to manufacturer's recommendations. They were validated as mycoplasma free using the MycoAlert detection kit from Lonza. The monoclonal anti-TFRC antibody clone DF1513 was purchased from Abcam and reconstituted in PBS for animal studies. Human holo-Tf was purchased from Sigma-Aldrich and used without further purification. ^{125}I was purchased from PerkinElmer. ^{68}Ga-citrate was manufactured and prepared for human use by the Radiopharmacy core facility at UCSF using previously described methods (15).

Radioiodination of human holo-Tf. Radiolabeling with ^{125}I was done in precoated Pierce iodination tubes (Thermo Fisher). Human holo-Tf (100 μg) was dispersed in 100 μl PBS solution and added to the precoated iodination tubes. Separately, a solution of 1 μl HCl (0.2 M), 2.5 μl phosphate buffer (0.5 M, pH 8), and 10 μl potassium iodide solution (1 mg/ml) was prepared. 1 mCi of ^{125}I was added into the iodination tubes, and the KI (aq.) solution was then mixed in the iodination tubes. After reaction for 15 minutes at room temperature, ^{125}I-labeled transferrin was purified using a PD10 column pre-equilibrated with 20 ml PBS solution. The purity of ^{125}I-transferrin was assessed with instant thin layer chromatography (iTLC), and was always found to be >98%.
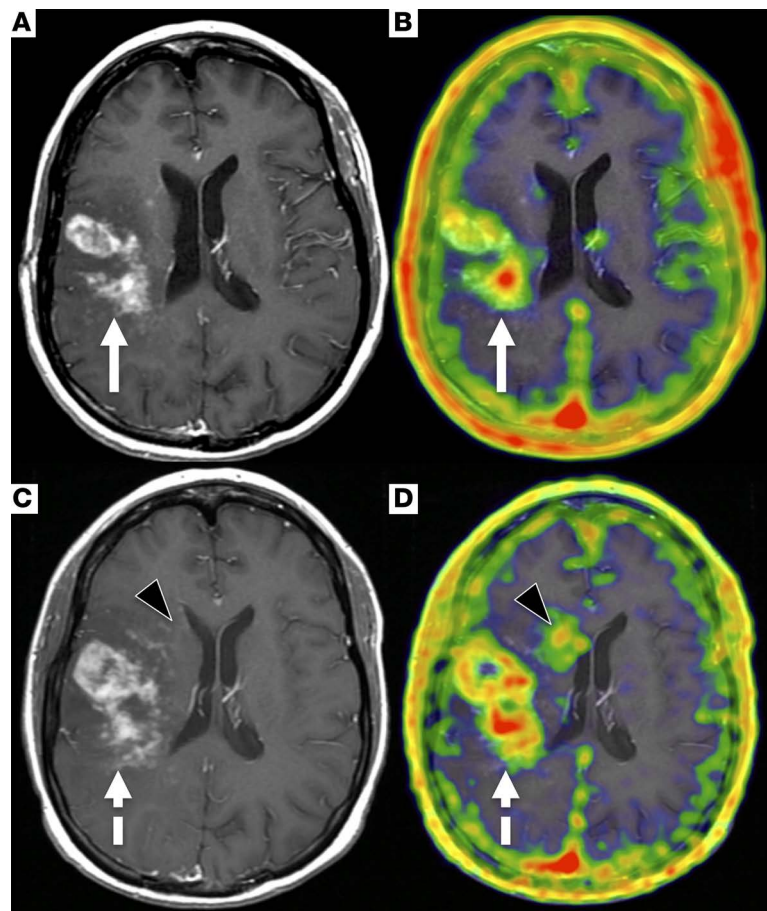
Figure 6. An example of tumor progression detected on MR with a corresponding increase in ^{68}Ga-citrate uptake in the tumor and a discrete region with faint enhancement. The initial PET/MR imaging was performed on a 36-year-old female with glioblastoma. The PET/MR was acquired 240 minutes after injection of 6.9 mCi (255.3 MBq) ^{68}Ga-citrate. T1-weighted post-contrast (**A**) and fused PET/MR (**B**) images demonstrate infiltrative right frontoparietal mass with corresponding ^{68}Ga-citrate uptake (SUV$_{max}$, 1.8, white arrows). The follow-up PET/MR was acquired 43 days later, and the imaging was performed 240 minutes after injection of 5.6 mCi (207.2 MBq) ^{68}Ga-citrate. Both T1-weighted post-contrast MR (**C**) and fused PET/MR (**D**) images show that the tumor has increased size and ^{68}Ga-citrate uptake (SUV$_{max}$, 3.2, dashed white arrows). A new focus of uptake in the right periventricular white matter with faint enhancement on the MR is also seen (black arrowheads).

In vitro binding assay. U87 MG or U251 cells were counted and plated at fixed cell concentrations between treatment arms in 6-well plates. Cells were treated with vehicle or 20 μg DF1513 for 15 minutes at 4°C (n = 4 per treatment arm). The cells were then treated with ^{125}I-Tf (~0.5 μCi per well) for 30 minutes. Unbound activity was removed, and the cells were washed twice with PBS. Cellular bound ^{125}I-Tf was harvested in 1 M NaOH (aq.). The cell-associated activity was expressed as the percent of total activity to which the cells were exposed. This value was further normalized to cell number (determined by counting cells in separate wells).

Animal studies. Four- to 6-week-old male *nu/nu* mice were purchased from Charles River. Mice were inoculated with 1×10^7 U87 MG cells subcutaneously into one flank in a 1:1 mixture (v/v) of media and Matrigel. Tumors were palpable within 14–21 days after injection. Animals were injected with DF1513 (100 μg) in PBS via the tail vein 24 or 48 hours prior to injection of ^{68}Ga-citrate. Tumor-bearing mice (n = 5 per treatment arm) received ~400 μCi ^{68}Ga-citrate in 100 μl NaCl (aq.) intravenously using a custom mouse tail vein catheter with a 28-gauge needle and 100- to 150-mm-long polyethylene microtubing (0.28-mm inner diameter × 0.64-mm outer diameter; Scientific Commodities Inc.). Animals were euthanized by CO_2 (gas) asphyxiation 2–6 hours after injection for biodistribution studies. Blood was accessed via cardiac puncture, and tissues, including the tumor, were harvested immediately following sacrifice. The blood and tissues were weighed and counted using a Wizard3 gamma counter (PerkinElmer) to assess
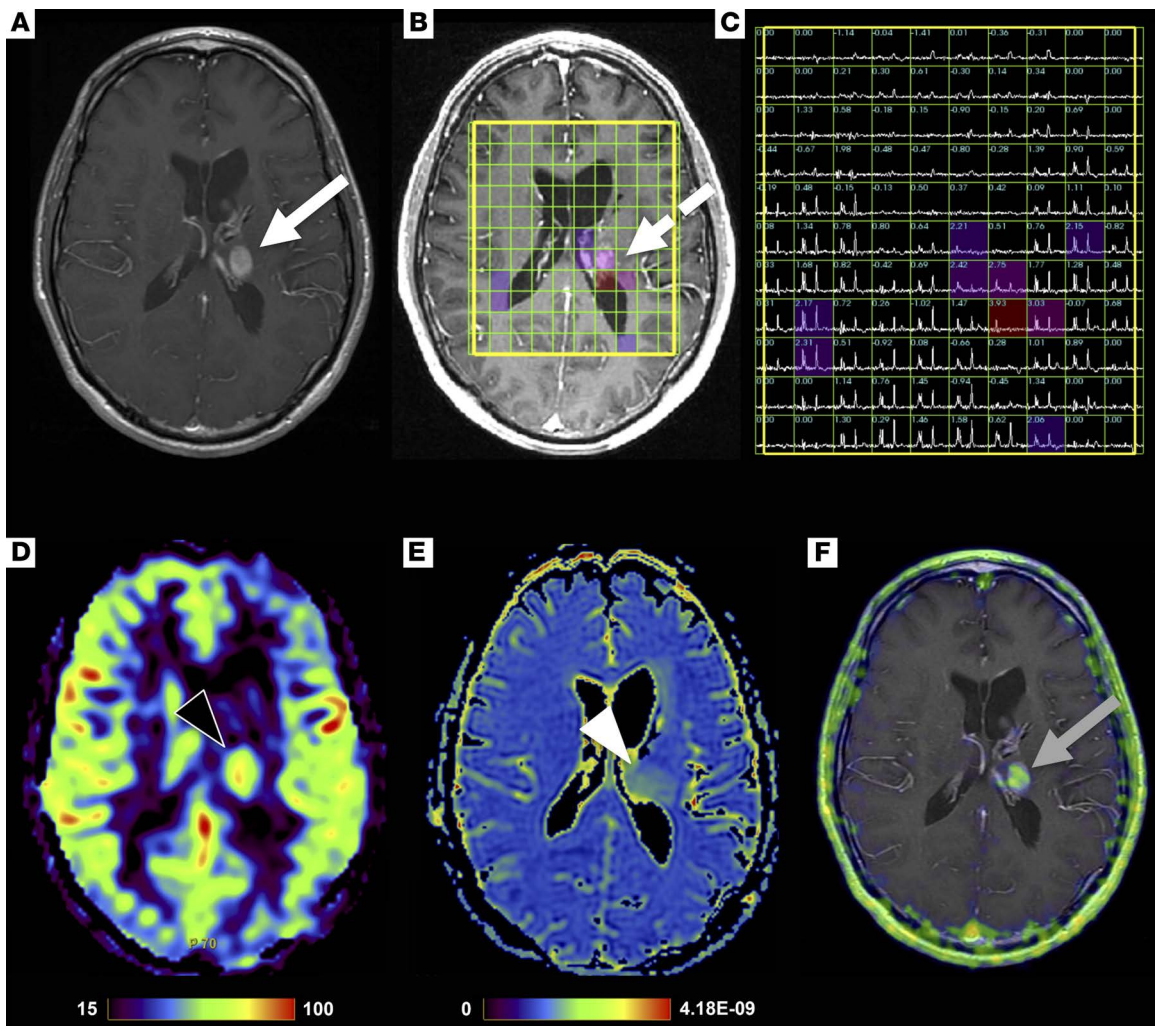
Figure 7. An example of a multimodality, multiparametric ⁶⁸Ga-citrate PET/MR examination showing overlap between the different parameters centered on the tumor. PET/MR imaging performed on a 32-year-old man with glioblastoma acquired 264 minutes after injection of 3.5 mCi (129.5 MBq) ⁶⁸Ga-citrate. T1-weighted post-contrast (**A**), 3D lactate-edited MR spectroscopy overlay (**B**), 3D MR spectra showing choline to *N*-acetylaspartate (NAA) index (**C**), arterial spin labeling cerebral blood flow map (**D**), apparent diffusion coefficient map (**E**), and fused PET/MR (**F**) images. Findings show a left thalamic enhancing lesion (white arrow) with abnormal metabolism (dashed white arrow), elevated perfusion (black arrowhead), no significant reduced diffusion (white arrowhead), and ⁶⁸Ga-citrate uptake with a SUV$_{max}$, 4.0 (gray arrow).

⁶⁸Ga concentration. Calibration with known amounts of ⁶⁸Ga was performed to determine the amount of activity in each organ. This activity was then decay corrected, and the percentage of the injected dose per gram (% ID/g) of tissue was calculated.

Patient characteristics and accrual. Patient inclusion criteria were as follows: (i) histologically confirmed WHO grade III or IV glioma; (ii) aged >18 years (iii); ability to undergo standard-of-care MRI, (iv) presence of at least 0.2-cm radiographic visible tumor on prior MRI; and (v) not pregnant. Patients were excluded if they (i) were not able to comply with follow-up procedures, (ii) were on any other experimental agents/clinical trials, or (iii) were unable to undergo MRI. Patient demographic information including age and sex were recorded, as well their tumor locations and histological grade (Supplemental Table 1).

Image acquisition. PET/MR examinations were performed on the SIGNA PET/MR scanner (GE Healthcare), which integrates a 3 Tesla MRI with time-of-flight PET. The imaging acquisitions were obtained simultaneously. ⁶⁸Ga-citrate uptake time ranged between 136 and 377 minutes (mean, 259 ± 75.6 minutes) after intravenous injection of ⁶⁸Ga-citrate (mean, 7 ± 2.0 mCi; range, 3.68–10.2 mCi). MR images were acquired using an 8-channel high-resolution brain coil. All images were acquired with patients holding their arms down by their sides.

A single-bed-position, 30-minute PET reconstruction through the head was generated using the list mode data set. PET reconstruction parameters were 192 × 192 matrix, 3-mm-thick filter, 28 subsets, 5 iterations with time-of-flight. Atlas-based attenuation correction was used to generate brain PET images.

A nuclear medicine physician in our research group (SCB) reviewed each PET on a standalone Advantage Windows workstation (GE Healthcare). A ratio of tumor SUV_{max} to SUV_{mean} blood pool and SUV_{max} tumor to SUV_{mean} white matter was calculated for each patient. Non-attenuation-corrected (NAC) PET, and attenuation-corrected (AC) PET and MR images were simultaneous reviewed. All positive lesions on AC images were confirmed on NAC. Additionally, NAC images and MR images were reviewed for any potential artifacts that could impact AC images. For assessment of uptake in normal structures, SUV_{mean} was recorded by drawing a 1-cm-diameter VOI in the right parietal white matter, the sagittal sinus, the right master muscle, and the right parotid gland (unless involved with tumor). If the tumor involved the right parietal white matter, the contralateral side was used.

Areas of abnormal PET uptake were considered positive if the ratio of signal in tumor versus adjacent white matter was at least 5:1. SUV_{max} and SUV_{peak} were recorded for each lesion by drawing a VOI that encompassed the entire PET lesion. SUV_{peak} was performed using a 5 mm diameter.

MR images were acquired through the brain using a standard-of-care brain tumor imaging protocol that included T1-weighted sequences, with fat saturation prior to and following intravenous gadolinium contrast administration, as well as 3D T2-weighted fluid attenuated inversion recovery (FLAIR) sequence. Additionally, DTI and MR spectroscopy were acquired. The size and location of each enhancing lesion were recorded. Two neuroradiologists in our research group (SC and JEV) reviewed the MR images.

Each scan was independently scored on a binary scale of absent or present by each radiologist for areas of abnormal contrast enhancement, radiotracer uptake, and discordance between the areas of contrast enhancement and PET. For patients with repeat exams, MR images were graded for progression as either absent or present.

Statistics. Preclinical data were analyzed using an unpaired, 2-tailed Student's *t* test with GraphPad Prism software. Changes at the 95% confidence level ($P < 0.05$) were interpreted as statistically significant. Descriptive statistics were calculated to analyze patient demographics, scan parameters, and imaging findings. Inter-rater reliability of PET/MR interpretation was assessed with Cohen's κ coefficient. Inter-rater reproducibility was interpreted as: 0–0.2, slight; 0.21–0.4, fair; 0.41–0.6, moderate; 0.61–0.8, substantial; and 0.81–1, near-perfect per previously described methods (32).

Study approval. All animal studies were conducted in compliance with the Institutional Animal Care and Use Committee of UCSF. This study was approved by the UCSF Institutional Review Board (IRB) and was compliant with the Health Insurance Portability and Accountability Act. Informed consent was obtained from all patients enrolled in the study.

Author contributions

Acknowledgments

Address correspondence to: Susan M. Chang, 400 Parnassus Avenue, San Francisco, California 94143, USA. Phone: 415.353.2383; Email: susan.chang@ucsf.edu. Or to: Michael J. Evans, 600 16th Street, N572C, San Francisco, California 94158, USA. Phone: 415.353.3442; Email: michael.evans@ucsf.edu.

1. Wen PY, et al. Updated response assessment criteria for high-grade gliomas: response assessment in neuro-oncology working group. *J Clin Oncol.* 2010;28(11):1963–1972.

2. Brandsma D, Stalpers L, Taal W, Sminia P, van den Bent MJ. Clinical features, mechanisms, and management of pseudoprogression in malignant gliomas. *Lancet Oncol.* 2008;9(5):453–461.

3. Herholz K. Brain tumors: an update on clinical PET research in gliomas. *Semin Nucl Med.* 2017;47(1):5–17.

4. Venneti S, et al. Glutamine-based PET imaging facilitates enhanced metabolic evaluation of gliomas in vivo. *Sci Transl Med.* 2015;7(274):274ra17.

5. Hygino da Cruz LC, Rodriguez I, Domingues RC, Gasparetto EL, Sorensen AG. Pseudoprogression and pseudoresponse: imaging challenges in the assessment of posttreatment glioma. *AJNR Am J Neuroradiol.* 2011;32(11):1978–1985.

6. Verma N, Cowperthwaite MC, Burnett MG, Markey MK. Differentiating tumor recurrence from treatment necrosis: a review of neuro-oncologic imaging strategies. *Neuro-oncology.* 2013;15(5):515–534.

7. Albert NL, et al. Response Assessment in Neuro-Oncology working group and European Association for Neuro-Oncology recommendations for the clinical use of PET imaging in gliomas. *Neuro-oncology.* 2016;18(9):1199–1208.

8. Langen KJ, Galldiks N, Hattingen E, Shah NJ. Advances in neuro-oncology imaging. *Nat Rev Neurol.* 2017;13(5):279–289.

9. Manz DH, Blanchette NL, Paul BT, Torti FM, Torti SV. Iron and cancer: recent insights. *Ann N Y Acad Sci.* 2016;1368(1):149–161.

10. McDowell KA, Riggins GJ, Gallia GL. Targeting the AKT pathway in glioblastoma. *Curr Pharm Des.* 2011;17(23):2411–2420.

11. Galvez T, et al. siRNA screen of the human signaling proteome identifies the PtdIns(3,4,5)P3-mTOR signaling pathway as a primary regulator of transferrin uptake. *Genome Biol.* 2007;8(7):R142.

12. Abe N, Inoue T, Galvez T, Klein L, Meyer T. Dissecting the role of PtdIns(4,5)P2 in endocytosis and recycling of the transferrin receptor. *J Cell Sci.* 2008;121(Pt 9):1488–1494.

13. Truillet C. Noninvasive measurement of mTORC1 signaling with [89]Zr-transferrin. *Clin Cancer Res.* 2017;5;23(12):3045–3052.

14. Masui K, Cloughesy TF, Mischel PS. Review: molecular pathology in adult high-grade gliomas: from molecular diagnostics to target therapies. *Neuropathol Appl Neurobiol.* 2012;38(3):271–291.

15. Behr SC, et al. A feasibility study showing [68Ga]citrate PET detects prostate cancer. *Mol Imaging Biol.* 2016;18(6):946–951.

16. Larson SM, et al. Common pathway for tumor cell uptake of gallium-67 and iron-59 via a transferrin receptor. *J Natl Cancer Inst.* 1980;64(1):41–53.

17. Aggarwal R, et al. Real-time transferrin-based PET detects MYC-positive prostate cancer. *Mol Cancer Res.* 2017;15(9):1221–1229.

18. Mari Aparici C, et al. Imaging hepatocellular carcinoma with ^{68}Ga-citrate PET: first clinical experience. *Mol Imaging.* 2017;16:1536012117723256.

19. Luttropp CA, Jackson JA, Jones BJ, Sohn MH, Lynch RE, Morton KA. Uptake of gallium-67 in transfected cells and tumors absent or enriched in the transferrin receptor. *J Nucl Med.* 1998;39(8):1405–1411.

20. Sohn MH, Jones BJ, Whiting JH, Datz FL, Lynch RE, Morton KA. Distribution of gallium-67 in normal and hypotransferrinemic tumor-bearing mice. *J Nucl Med.* 1993;34(12):2135–2143.

21. Aloj L, Carson RE, Lang L, Herscovitch P, Eckelman WC. Measurement of transferrin receptor kinetics in the baboon liver using dynamic positron emission tomography imaging and [18F]holo-transferrin. *Hepatology.* 1997;25(4):986–990.

22. Holland JP, Evans MJ, Rice SL, Wongvipat J, Sawyers CL, Lewis JS. Annotating MYC status with 89Zr-transferrin imaging. *Nat Med.* 2012;18(10):1586–1591.

23. Ciechanover A, Schwartz AL, Dautry-Varsat A, Lodish HF. Kinetics of internalization and recycling of transferrin and the transferrin receptor in a human hepatoma cell line. Effect of lysosomotropic agents. *J Biol Chem.* 1983;258(16):9681–9689.

24. Iacopetta BJ, Morgan EH. The kinetics of transferrin endocytosis and iron uptake from transferrin in rabbit reticulocytes. *J Biol Chem.* 1983;258(15):9108–9115.

25. O'Donnell KA, et al. Activation of transferrin receptor 1 by c-Myc enhances cellular proliferation and tumorigenesis. *Mol Cell Biol.* 2006;26(6):2373–2386.

26. Doran MG, et al. Applying [89]Zr-transferrin to study the pharmacology of inhibitors to BET bromodomain containing proteins. *Mol Pharm.* 2016;13(2):683–688.

27. Evans MJ, et al. Imaging tumor burden in the brain with 89Zr-transferrin. *J Nucl Med.* 2013;54(1):90–95.

28. Chen W, et al. 18F-FDOPA PET imaging of brain tumors: comparison study with 18F-FDG PET and evaluation of diagnostic accuracy. *J Nucl Med.* 2006;47(6):904–911.

29. Rapp M, et al. Diagnostic performance of 18F-FET PET in newly diagnosed cerebral lesions suggestive of glioma. *J Nucl Med.* 2013;54(2):229–235.

30. Chen W, et al. Imaging proliferation in brain tumors with 18F-FLT PET: comparison with 18F-FDG. *J Nucl Med.* 2005;46(6):945–952.

31. Yang J, et al. 2017. Quantitative evaluation of atlas-based attenuation correction for brain PET in an integrated time-of-flight PET/MR imaging system. *Radiology.* 2017;284(1):169–179.

32. Landis JR, Koch GG. The measurement of observer agreement for categorical data. *Biometrics.* 1977;33(1):159–174.